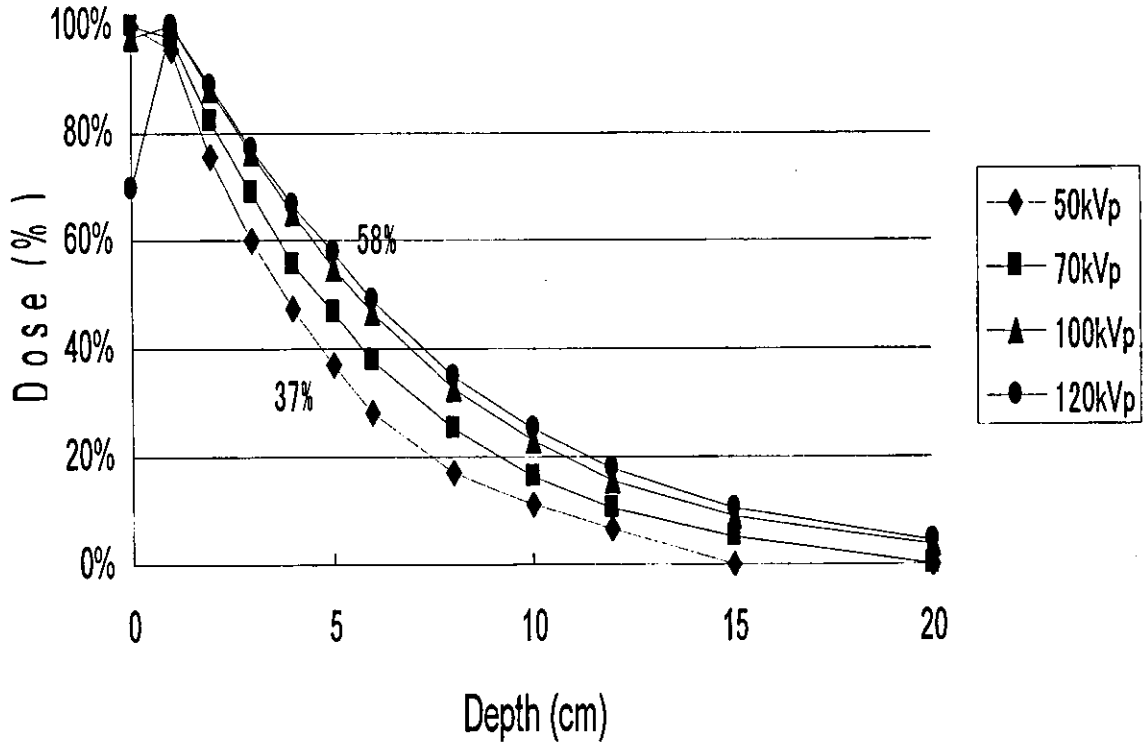

Fig. 4. Percent depth dose curves according to kilovoltage peak of fluoroscope. Diamonds, 50 kV; squares; 70 kV, triangles; 100 kV; circles, 120 kV.

Because RTRT usually requires two sets of fluoroscopy, the maximal dose possible to deliver to the skin surface is two times the dose at the skin surface from one fluoroscope. Usually, the two diagnostic beams do not overlap at the skin surface. However, they could overlap if treating a tumor very close to the skin surface. With the expected RT times needed for IMRT plus RTRT and the exposure parameters required for sufficient image quality, the patient exposure could be unacceptable.

A normal (four fields), 2-Gy, static field treatment is

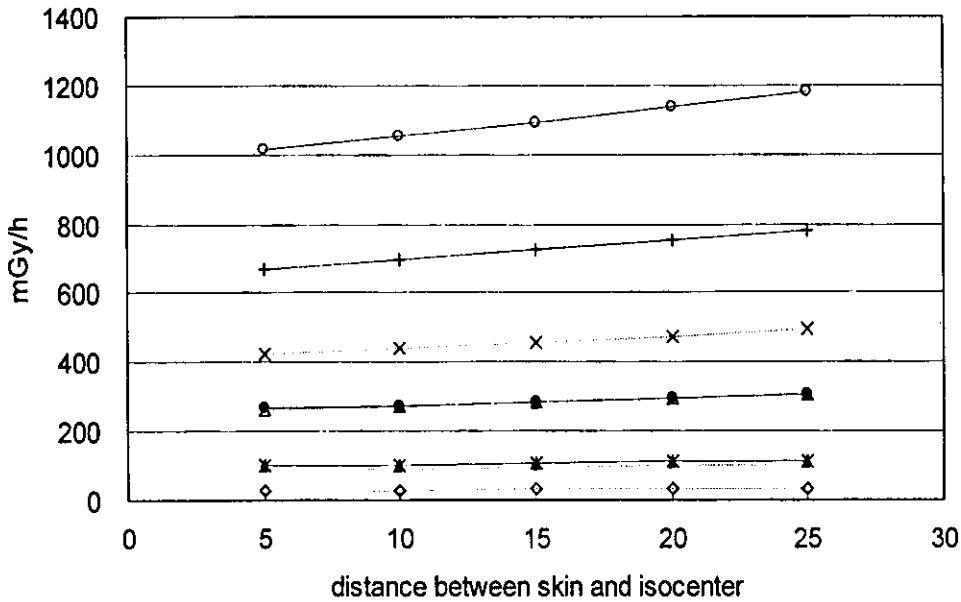

Fig. 5. Relationship between distance from surface to isocenter and surface dose rate from one fluoroscope. Diamonds, 50 kVp, 1.2 ms; asterisks, 50 kVp, 4.0 ms; squares, 70 kVp, 1.2 ms; black circles, 70 kVp, 1.4 ms; triangles, 100 kVp, 1.2 ms; plus signs, 100 kVp, 1.4 ms; crosses, 120 kVP, 1.2 ms; white circles, 120 kVp, 1.4 ms.

≤300 MU approximately. At 300 MU/min and a 25% duty cycle, this would equal 4 min of surveillance time or a skin dose of ~8 cGy (highest case, 120 kVP and 4 ms [Fig. 5], 4 min/60 min × 1.2 Gy/h). If IMRT increases the monitor unit (MU) by a factor of 3–5, the treatment time should be only 12–20 min; however, the fluoroscopic dose becomes worrisome, not so much at the skin but at depth, for which the PDD may not be insignificant. In practice, we have noted that intrafractional fluctuation of tumor motion is often so large that the table position must be adjusted several times by additional fluoroscopic examination (8). In that case, the fluoroscopic dose could extend to 30 min.

In interventional neuroradiology, advances in insertion techniques and catheter materials have increased the acceptable exposure time of diagnostic radiography. The unexpectedly high doses used in modern interventional radiology have raised concerns about radiation safety and protection (18). The results of the present study have confirmed that it is also important to reduce the radiation dose from fluoroscopic exposure during RT. A reduction of the field size is important, but not the perfect answer, because the same area of skin will receive the same dose every day during RTRT. Sharp *et al.* (24) have found that various prediction models, such as a linear model or neural network model, can help reduce the pulse rate to <30 Hz. They considered 14 lung tumor cases in which the peak-to-peak motion was >8 mm and compared the localization error using linear prediction, neural network prediction, and Kalman filtering against a system that used no prediction. They found that by using prediction, the root mean squared error between the predicted and actual three-dimensional (3D) motion was improved for all latencies and all imaging rates evaluated. A reduction in the source-to-detector distance is also useful to reduce the amount of exposure. The attachment of the X-ray tubes and cameras to the gantry head of the linear accelerator can reduce the source-to-detector distance significantly (17). The amount of reduction in the absorbed dose will be about one-third of that of our system, providing that the same dose is required at the surface of the image intensifier. Amorphous silicon directors may reduce the dose required to obtain an image with the same time resolution; the absorbed dose will be further reduced. Changing the fluoroscopy angle according to changes in the therapeutic beam angle beam may also help to reduce the dose to the same skin surface. The shortcoming of the gantry-mounted imaging units may be their inability to use noncoplanar irradiation techniques and the difficulty in maintaining imaging unit accuracy. Also, the X-ray tubes and image detectors can be an obstacle during non-RTRT. Magnetic detection of the metallic marker in the body can eliminate the requirement for fluoroscopic exposure and is also expected to be an alterative to the fluoroscopic detection of internal fiducial markers (25).

We have adapted several approaches to reduce the amount of exposure from fluoroscopy to synchronize RTRT and IMRT. First, software was designed that allows the use of one instead of two sets of fluoroscopy for tracking after registration between the 3D coordinates and the two-dimensional projected coordinates of the marker on one fluoroscopic image. The shortcoming of this method is that two-dimensional projection does not provide information about the third dimension; thus, we have not yet used the two-dimensional projection method in a clinical situation. Second, the pulse rate is now changeable from 30 Hz to 15, 10, 5, and 2 Hz. If the tumor is moving slowly, the lower pulse rate can be used. Third, a 3D trajectory of the tumor is obtained before actual treatment and is used to select the best position for tracking each day to improve gating efficiency. We plan to include the 3D dose distribution of the fluoroscopic beam in our treatment planning system to combine it with the dose distribution of the therapeutic beams. Details of these developments will be described elsewhere.

CONCLUSION

The absolute dose and depth–dose distribution of fluoroscopy in the RTRT system showed that synchronization of RTRT and IMRT may result in an unacceptably high radiation dose to the skin surface and possibly to the deep tissues. The synchronization of RTRT and IMRT requires improvement to reduce fluoroscopic exposure.

REFERENCES

1. Shirato H, Harada T, Harabayashi T, *et al.* Feasibility of insertion/implantation of 2.0-mm-diameter gold internal fiducial markers for precise setup and real-time tumor tracking in radiotherapy. *Int J Radiat Oncol Biol Phys* 2003;56:240–247.
2. Shimizu S, Shirato H, Kitamura K, *et al.* Use of an implanted marker and real-time tracking of the marker for the positioning of prostate and bladder cancers. *Int J Radiat Oncol Biol Phys* 2000;48:1591–1597.
3. Kitamura K, Shirato H, Shimizu S, *et al.* Registration accuracy and possible migration of internal fiducial gold marker implanted in prostate and liver treated with real-time tumor-tracking radiation therapy (RTRT). *Radiother Oncol* 2002;62: 275–281.
4. Kaatee RS, Olofsen MJ, Verstraate MB, *et al.* Detection of organ movement in cervix cancer patients using a fluoroscopic electronic portal imaging device and radiopaque markers. *Int J Radiat Oncol Biol Phys* 2002;54:576–583.
5. Poggi MM, Gant DA, Sewchand W, *et al.* Marker seed migration in prostate localization. *Int J Radiat Oncol Biol Phys* 2003;56:1248–1251.
6. Shimizu S, Shirato H, Ogura S, *et al.* Detection of lung tumor movement in real-time tumor-tracking radiotherapy. *Int J Radiat Oncol Biol Phys* 2001;51:304–310.
7. Kubo HD, Wang L. Introduction of audio gating to further reduce organ motion in breathing synchronized radiotherapy. *Med Phys* 2002;29:345–350.
8. Seppenwoolde Y, Shirato H, Kitamura K, *et al.* Precise and real-time measurement of 3D tumor motion in lung due to breathing and heartbeat, measured during radiotherapy. *Int J Radiat Oncol Biol Phys* 2002;53:822–834.

9. Harada T, Shirato H, Ogura S, *et al.* Real-time tumor-tracking radiation therapy for lung carcinoma by the aid of insertion of a gold marker using bronchofiberscopy. *Cancer* 2002;95:1720–1727.
10. Kitamura K, Shirato H, Seppenwoolde Y, *et al.* Tumor location, cirrhosis, and surgical history contribute to tumor movement in the liver, as measured during stereotactic irradiation using a real-time tumor-tracking radiotherapy system. *Int J Radiat Oncol Biol Phys* 2003;56:221–228.
11. Minohara S, Kanai T, Endo M, *et al.* Respiratory gated irradiation system for heavy-ion radiotherapy. *Int J Radiat Oncol Biol Phys* 2000;47:1097–1103.
12. Shirato H, Shimizu S, Kitamura K, *et al.* Four-dimensional treatment planning and fluoroscopic real-time tumor tracking radiotherapy for moving tumor. *Int J Radiat Oncol Biol Phys* 2000;48:435–442.
13. Vedam SS, Keall PJ, Kini VR, *et al.* Acquiring a four-dimensional computed tomography dataset using an external respiratory signal. *Phys Med Biol* 2003;48:45–62.
14. Ford EC, Mageras GS, Yorke E, *et al.* Respiration-correlated spiral CT: A method of measuring respiratory-induced anatomic motion for radiation treatment planning. *Med Phys* 2003;30:88–97.
15. Brock KK, Hollister SJ, Dawson LA, *et al.* Technical note: Creating a four-dimensional model of the liver using finite element analysis. *Med Phys* 2002;29:1403–1405.
16. Shirato H, Shimizu S, Kunieda T, *et al.* Physical aspects of a real-time tumor-tracking system for gated radiotherapy. *Int J Radiat Oncol Biol Phys* 2000;48:1187–1195.
17. Neicu T, Shirato H, Seppenwoolde Y, *et al.* Synchronized moving aperture radiation therapy (SMART): Average tumour trajectory for lung patients. *Phys Med Biol* 2003;48:587–598.
18. Kemerink GJ, Frantzen MJ, Oei K, *et al.* Patient and occupational dose in neurointerventional procedures. *Neuroradiology* 2002;44:522–528.
19. Gkanatsios NA, Huda W, Peters KR. Adult patient doses in interventional neuroradiology. *Med Phys* 2002;29:717–723.
20. Joint Working Party of the British Institute of Radiology and the Hospital Physicists' Association. Central axis depth dose data for use in radiotherapy. *Br J Radiol* 1996;(Suppl. 25).
21. Jennings WA, Harrison RM. X-rays: Half-value thickness range 0.01–8.0 mm Al. *Br J Radiol* 1983;17:1–7.
22. Harrison RM. Central-axis depth-dose data for diagnostic radiology. *Phys Med Biol* 1981;26:657–670.
23. Fetterly KA, Gerbi BJ, Alaei P, *et al.* Measurement of the dose deposition characteristics of x-ray fluoroscopy beams in water. *Med Phys* 2001;28:205–209.
24. Sharp G, Jiang SB, Shimizu S, *et al.* Prediction of respiratory tumor motion for real-time image-guided radiotherapy. *Phys Med Biol* 2004;49:425–440.
25. Seiler PG, Blattmann H, Kirsch S, *et al.* A novel tracking technique for the continuous precise measurement of tumour positions in conformal radiotherapy. *Phys Med Biol* 2000;45:N103–N110.

Int. J. Radiation Oncology Biol. Phys., Vol. 58, No. 4, pp. 1177–1183, 2004

0360-3016/04/$–see front matter

ELSEVIER

doi:10.1016/j.ijrobp.2003.08.034

CLINICAL INVESTIGATION **Brain**

INTEGRATION OF FUNCTIONAL BRAIN INFORMATION INTO STEREOTACTIC IRRADIATION TREATMENT PLANNING USING MAGNETOENCEPHALOGRAPHY AND MAGNETIC RESONANCE AXONOGRAPHY

HIDEFUMI AOYAMA, M.D., PH.D.,* KYOUSUKE KAMADA, M.D., PH.D.,†
HIROKI SHIRATO, M.D., PH.D.,* FUMIYA TAKEUCHI, PH.D.,‡ SHINYA KURIKI, PH.D.,‡
YOSHINOBU IWASAKI, M.D., PH.D.,† AND KAZUO MIYASAKA, M.D., PH.D.*

Departments of *Radiology and †Neurosurgery, Hokkaido University Graduate School of Medicine; ‡Research Institute of Applied Electricity, Hokkaido University, Sapporo, Japan

Purpose: To minimize the risk of neurologic deficit after stereotactic irradiation, functional brain information was integrated into treatment planning.

Methods and Materials: Twenty-one magnetoencephalography and six magnetic resonance axonographic images were made in 20 patients to evaluate the sensorimotor cortex (n = 15 patients, including the corticospinal tract in 6), visual cortex (n = 4), and Wernicke's area (n = 2). One radiation oncologist was asked to formulate a treatment plan first without the functional images and then to modify the plan after seeing them. The pre- and postmodification values were compared for the volume of the functional area receiving ≥15 Gy and the volume of the planning target volume receiving ≥80% of the prescribed dose.

Results: Of the 21 plans, 15 (71%) were modified after seeing the functional images. After modification, the volume receiving ≥15 Gy was significantly reduced compared with the values before modification in those 15 sets of plans (p = 0.03). No statistically significant difference was found in the volume of the planning target volume receiving ≥80% of the prescribed dose (p = 0.99). During follow-up, radiation-induced necrosis at the corticospinal tract caused a minor motor deficit in 1 patient for whom magnetic resonance axonography was not available in the treatment planning. No radiation-induced functional deficit was observed in the other patients.

Conclusion: Integration of magnetoencephalography and magnetic resonance axonography in treatment planning has the potential to reduce the risk of radiation-induced functional dysfunction without deterioration of the dose distribution in the target volume. © **2004 Elsevier Inc.**

Radiosurgery, Magnetoencephalography, Axon, Function, Arteriovenous malformation.

INTRODUCTION

One of the advantages of stereotactic irradiation (STI) over surgical resection in the treatment of brain diseases is that STI is an easier and safer method of accessing areas deep in the brain, as well as those located in the vicinity of the functional brain cortex. Permanent radiation injury, known as radiation necrosis, is not a common consequence of STI. However, once necrosis occurs in certain areas of the brain responsible for motor function, visual function, comprehension, or speech production, it results in permanent neurologic deficits (1–4). The development of radiation necrosis is related to the dose of radiation received. Considering that neuronal fibers are serial in structure, the severity of the neurologic deficit is expected to be related to factors such as the maximal radiation dose administered to functional brain areas, as well as the volume of the area exposed to more than the threshold dose of radiation (5, 6). Although the threshold dose of radiation required to develop radiation necrosis has not been fully investigated, some clinical and experimental data have indicated that the threshold single dose lies within the range of 10–15 Gy (3, 4, 7).

Recently, imaging modalities that enable the identification of functional brain areas have emerged as clinically significant (8–18). Magnetoencephalography (MEG) is used to detect the magnetic field associated with intracranial neuronal electric activity. In practice, it has been used to identify the sensorimotor, visual, and Wernicke's speech cortices (8, 10–12). Magnetic resonance (MR) axonography or anisotropic diffusion-weighted MRI (ADWI) is a method that visualizes the

Reprint requests to: Hidefumi Aoyama, M.D., Ph.D., Department of Radiology, Hokkaido University Graduate School of Medicine, North-15 West-7, Kita-ku, Sapporo 060-8638, Japan. Tel: (+81) 11-716-1161; Fax: (+81) 11-706-7876; E-mail: hao@radi.med.hokudai.ac.jp

Presented in part at the American Society for Therapeutic Radiology and Oncology (ASTRO) Annual Meeting, New Orleans, LA, October 2002.

Received Feb 4, 2003, and in revised form Aug 11, 2003. Accepted for publication Aug 15, 2003.

Table 1. Patient characteristics and results

Pt. No.	Disease	Age (y)	Follow-up (mo)	Modality	Identified functional area	RT dose (Gy)/ fraction (n)	D_{max} (Gy) Functional information		V_{10} (cm^3) Functional information		V_{15} (cm^3) Functional information	
							Yes	No	Yes	No	Yes	No
1	Met	59	29	MEG	Motor cortex	35/4	16.3	18.7	0.9	6.2	0.2	5.3
2	Met	82	4	MEG	Visual cortex	35/4	18.7	19.2	1.7	3.7	0.9	5.5
3	Met	75	5	MEG	Motor cortex	35/4	18.5	19.1	2.46	3.72	1.02	3.48
	Met			MEG	Visual cortex	35/4	11.1	18.5	0.09	0.97	0	0.89
4	AVM	11	31	MEG	Motor cortex	22.5/1	7.0	11.3	0	0.34	0	0
5	AVM	41	23	MEG	Motor cortex	20/1	16.0	16	0.32	0.32	0.16	0.16
6	AVM	26	37	MEG	Motor cortex	35/4	17.4	20.3	2.68	7.68	0.7	3.96
7	AVM	45	31	MEG	Motor cortex	35/4	7.5	9.6	0	0.11	0	0
8	AVM	40	34	MEG	Motor cortex	25/1	9.9	10.1	0	0	0	0
9	AVM	21	27	MEG	Visual cortex	20/4	6.1	9	0.11	0.11	0	0
10	AVM	29	21	MEG	Wernicke's area	25/1	3.7	3.7	0	0	0	0
11	Met	64	8	MEG	Motor cortex	25/1	25.0	26	3.06	4.5	1.98	3.5
12	Met	64	20	MEG	Motor cortex	35/4	16.1	16.1	0.76	0.76	0	0
13	AVM	45	18	MEG+AX	Motor cortex and CST	35/4	12.4	13.8	1.69	1.88	2.6	3.1
14	AVM	60	3	MEG+AX	Motor cortex and CST	35/4	8.0	11.7	1.09	1.59	1.4	0.5
15	AVM	27	13	MEG	Visual cortex	20/1	2.0	2	0	0	0	0
16	AVM	12	9	MEG+AX	Motor cortex and CST	15/1	15.9	15.9	4.68	4.68	0.36	0.36
17	AVM	44	8	MEG	Wernicke's area	35/4	7.3	9.7	0	0	0	0
18	AVM	51	6	MEG+AX	Motor cortex and CST	35/4	0.0	0	0	0	0	0
19	AVM	65	6	MEG+AX	Motor cortex and CST	33/4	14.8	17.2	0	0	0	0
20	AVM	58	6	MEG+AX	Motor cortex and CST	35/4	17.4	18.3	0.35	0.49	0.07	0.14

Abbreviations: Pt. No. = patient number; RT = radiotherapy; D_{max} = maximal dose within functional area converted into single fraction schedule by linear quadratic model; V_{10} or V_{15} = volume of functional area receiving ≥ 10 Gy or ≥15 Gy; Met = metastasis; MEG = magnetoencephalography; AVM = arteriovenous malformation; AX = MR axonography; CST = corticospinal tract.

axonal pathway in the brain. ADWI applies three-orthogonal diffusion gradient pulses and can clearly demonstrate neuronal fibers perpendicular to a diffusion gradient as a hyperintense area. Theoretically, all the subcortical tracts that run in the cranial–caudal direction become hyperintense in the AP diffusion gradient; however, previous reports on ADWI have suggested that the hyperintense areas might consist mainly of the corticospinal tract (16–18).

Integration of the three-dimensional (3D) configuration of functional brain areas into conformal radiotherapy planning using MEG and ADWI may minimize the risk of developing symptomatic adverse effects due to radiation necrosis at the functional brain area. In this study, we evaluated the potential contribution of integrating functional information into radiotherapy planning by dose–volume statistics to reduce the risk of symptomatic radiation necrosis. Preliminary clinical outcomes are also reported.

METHODS AND MATERIALS

Twenty patients (8 females and 12 males, median age, 45 years; range, 11–82 years) with intracranial disease located near or within the functional cortex or corticospinal tract were included in this study. The patient characteristics are listed in Table 1. Five patients had brain metastases and 15 had arteriovenous malformations (AVMs). One of the patients with metastases underwent STI for two lesions; thus, 21 lesions were included. Functional brain areas were identified by MEG in all 21 areas of the 20 patients. Six recent cases in which the lesions were close to the corticospinal tract pathway were evaluated using ADWI as well. Follow-up ranged from 3 to 35 months (mean, 12 months).

The MEG studies were performed in a magnetically shielded room with a 204-channel whole-head biomagnetometer (VectorView, 4D-Neuroimage, San Diego, CA). The spatial resolution of MEG to detect the location of functional cortex is considered to be <5 mm (8–12). For the identification of the sensorimotor cortex in 15 patients, a somatosensory mapping protocol was used in which the median and tibial nerves contralateral to the side of the lesion were stimulated at the wrist and ankles, respectively, with 0.2-ms constant-current pulses. For the primary visual cortex mapping in 4 patients (Fig. 1), the visually evoked field was measured by standard pattern shift stimulation. Wernicke's area was identified by a simple object-naming task in 2 right-handed patients (Fig. 2). In the evaluation of the corticospinal tract using ADWI, hyperintense areas with an intensity 1.6 times greater than that of normal white matter in the AP diffusion gradient were considered as part of the corticospinal tract (Fig. 3). Anatomic, ADWI experiments were performed during MRI investigation using a 1.5-T whole-body MRI scanner with echo-planner capabilities and a standard whole-head transmit-receiver coil (Magnetom Vision, Siemens AG, Erlangen, Germany). Four sessions of multislice, single-shot, spin-echo, echo-planar ADWI (TE, 87 ms; 128 × 128 matrix; 19 slices) were performed with a b value of 1000 s/mm^2. After the raw data of

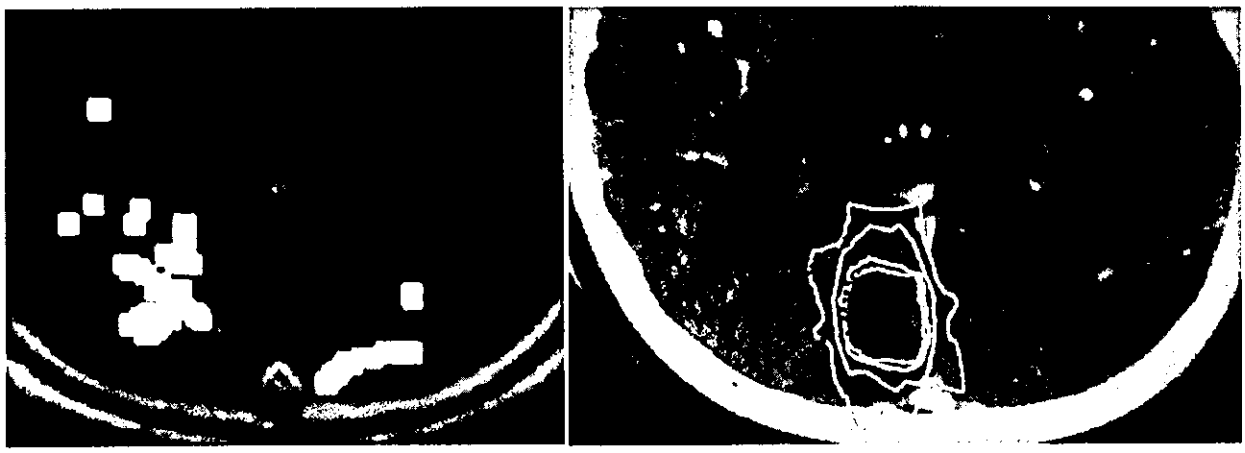

(a) (b)

Fig. 1. Brain metastasis near primary visual cortex (Patient 2). (a) Enhanced MRI with dipoles for primary visual cortex showing normally located left primary visual cortex and dislocated right primary visual cortex by metastasis. (b) Planning target volume (black solid line), primary visual cortex (black dotted line), and isodose lines (white lines, 90%, 80%, 50%, and 30% from inside out).

each ADWI session were two-dimensionally reconstructed, all four sessions of ADWI were averaged. The diffusion gradients were applied sequentially in three orthogonal directions to generate three sets of transverse ADW images to visualize the tract orientation. Because the corticospinal tract was theoretically expected to be the most hyperintense area in the AP diffusion gradient, we took as the corticospinal tract those hyperintense areas having intensity 1.6 times greater than the normal white matter. Anatomic 3D-MRI data of each patient's head was obtained, resulting in 128 sequential, 1.8-mm-thick, axial slices with a resolution of 256 × 256 pixels in a field of view of 300 mm. Data from Both the MEG dipole and the ADWI were integrated into an anatomic 3D-MR image, herein referred to as function-integrated MRI.

The MRI scan can be registered with the CT image using a CT-MRI fusion system (EV pro, Hitachi Medico, Tokyo), as described in detail previously (19). The anatomic CT scan for radiation planning was conducted using a conventional CT

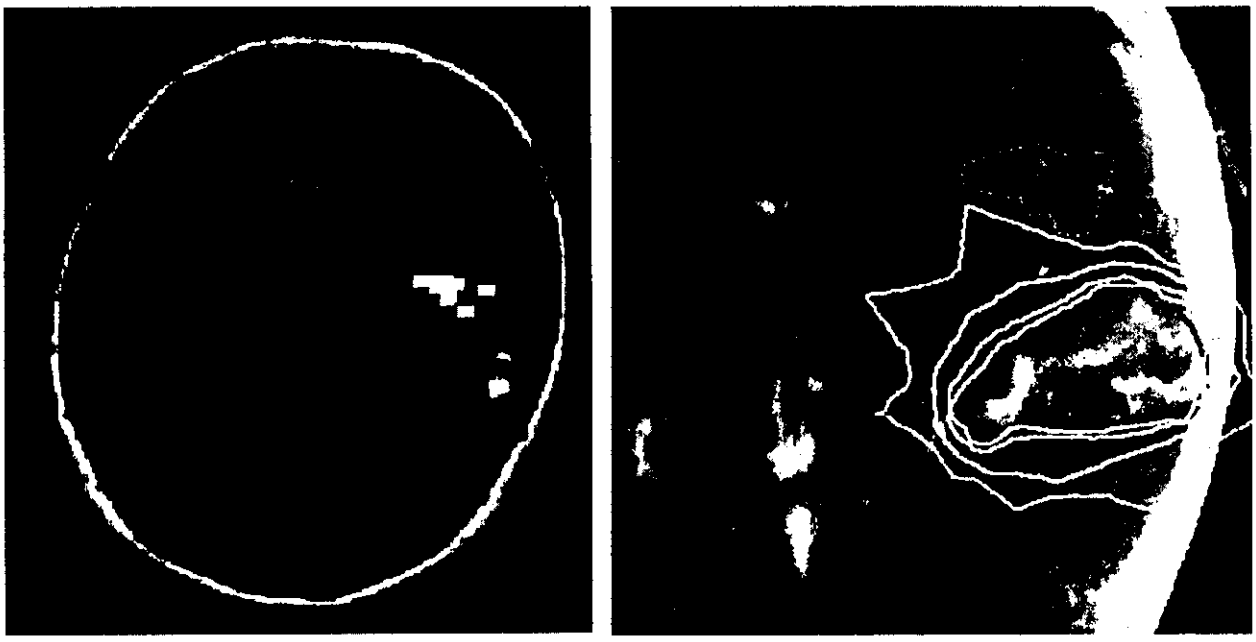

(a) (b)

Fig. 2. Arteriovenous malformation close to Wernicke's area (Patient 17). (a) T_1-weighted MRI with dipoles of magnetoencephalography. (b) Planning target volume (black solid line), Wernicke's area (black dotted line), and isodose lines (white lines, 90%, 80%, 50%, and 30% from inside out).

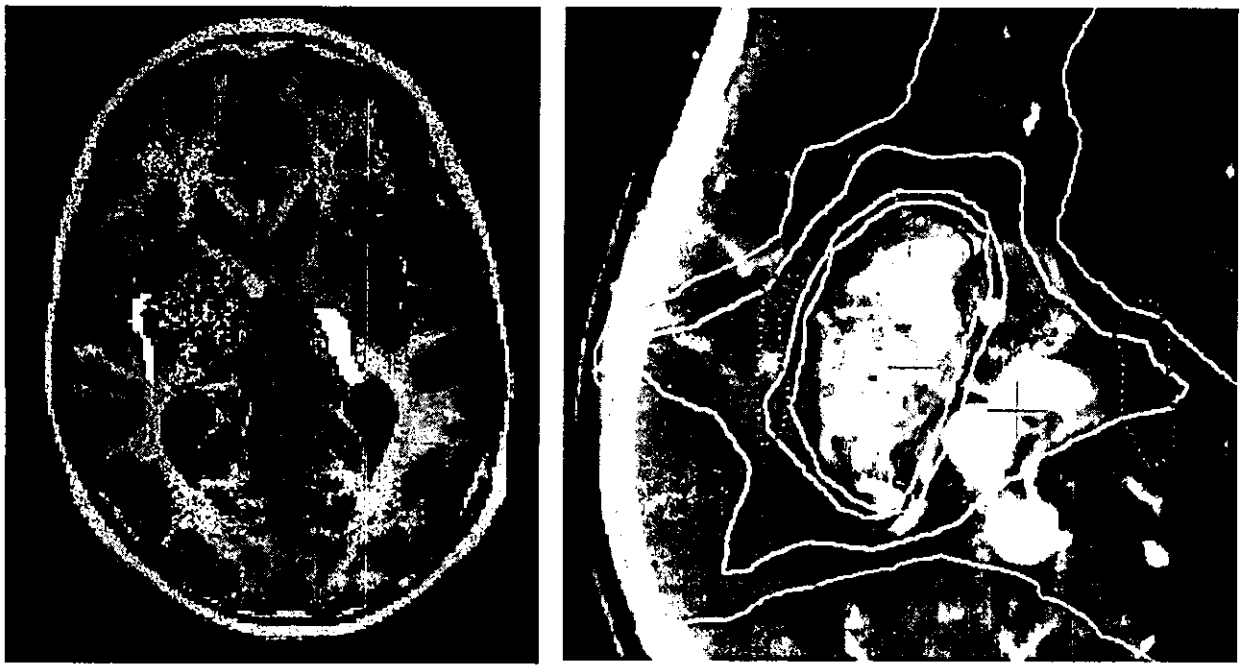

(a) (b)

Fig. 3. Arteriovenous malformation (AVM) close to corticospinal tract (Patient 16). (a) MR axonography showing right corticospinal tract dislocated by large AVM. (b) Planning target volume (black solid line), corticospinal tract (black dotted line), and isodose lines (white lines, 90%, 80%, 50%, and 30% from inside out).

machine (Sfida, SCT-7000TX/TH, Shimazu, Kyoto) with slice thickness of 3 or 5 mm and a matrix size of 256 × 256 with a field of view of 280 mm. In brief, registration of the CT and MRI scans can be conducted on the basis of four or more anatomic landmarks (e.g., the bilateral cochlea, top of the basilar artery, anterior commissure). After the registration, the contoured region-of-interest, such as the tumor or organs at risk on MRI, is automatically superimposed on the relevant CT image. In the same manner, after the registration of the function-integrated MRI with the CT image, the functional area was contoured on MRI and then superimposed on the relevant CT images. The CT images with the contours of the tumors, anatomic organs at risk, and functional area (i.e., function-integrated CT images) can be transferred to a 3D-RTP system (Focus, CMS, St. Louis, MO) and used for dose calculation with inhomogeneity correction. STI was performed with a 6-MV linear accelerator-based stereotactic system (Clinac 2300 C/D, Varian, CA) using treatment parameters transferred via Ethernet. The setup accuracy of the system was estimated to be ±1 mm.

In this study, the treatment plans were first created using conventional MRI-CT fusion images without functional data by one radiation oncologist who was unaware of the information regarding the functional brain areas. After the radiation oncologist had completed the treatment plans, they were modified using function-integrated CT images. We evaluated the influence of the integration of functional information into the planning by comparing the dose–volume statistics between the two consecutive plans for the same patient. The final treatment plans formulated using function-integrated CT were chosen for actual treatment.

Radiation was delivered radiosurgically in a single session to five lesions ranging in isocentric doses from 20 to 25 Gy (median, 20 Gy). Ten other lesions were treated with hypofractionated STI using 20–35 Gy (median, 35 Gy) at the isocenter in four fractions. The planning target volume (PTV) was covered with an 80–90% isodose surface. To simplify the evaluation, each schedule of hypofractionated dose was converted into a single fraction schedule using a linear-quadratic model with an α/β ratio of 2 for normal tissue. The maximal dose (D_{max}) to the functional area and the volume of the functional area receiving ≥10 Gy (V_{10}) and ≥15 Gy (V_{15}) were used to evaluate the effect on the functional area. The dose that 95% of the PTV received and the amount of the PTV receiving ≥80% of the prescribed dose were used to evaluate the effect on the target volume. Student's t test was used for the comparison. Values of $p < 0.05$ were considered to indicate statistical significance.

RESULTS

Dose–volume statistics

The functional cortex was successfully identified in all 21 regions using MEG. The corticospinal tract pathway was also well identified using ADWI in all 6 patients examined. Of the 21 plans, 15 (71%) were judged to have been modified using the function-integrated CT images and only 6 (29%) remained unchanged.

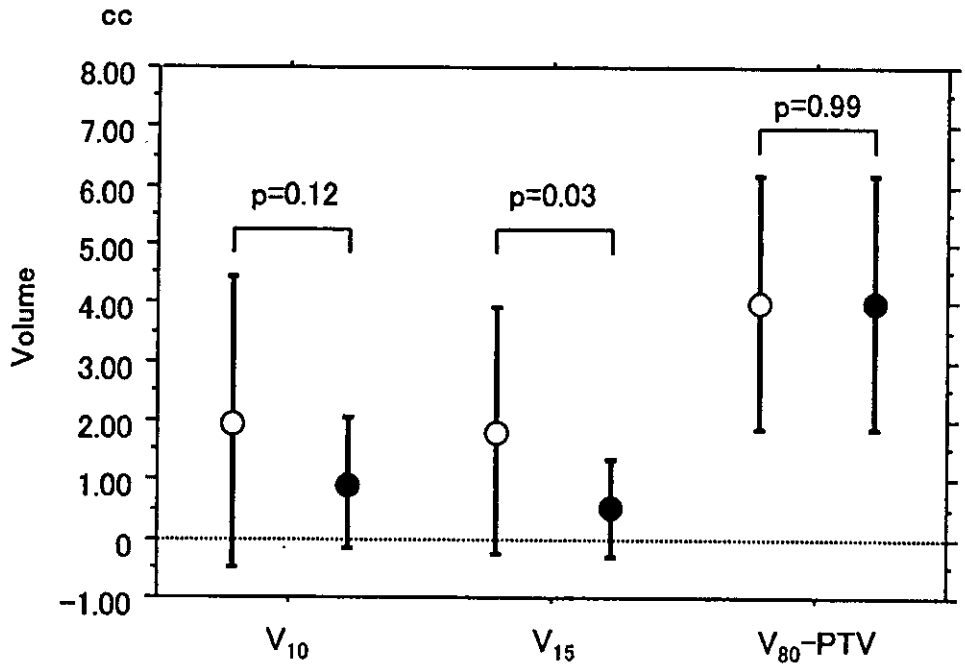

Fig. 4. Volume of functional area receiving ≥10 Gy or ≥15 Gy and amount of planning target volume (PTV) receiving ≥80% of prescribed dose before (white circles) and after (black circles) modification in 15 sets of plans that were changed after seeing the functional information.

In the 15 lesions for which the plan was modified, the D_{max}, V_{10}, and V_{15} of the functional area after the modification were consistently reduced compared with the plan without functional information. The mean D_{max}, V_{10}, and V_{15} before modification was 15.5 Gy, 2.1 cm^3, and 1.8 cm^3, respectively, and was reduced to 13 Gy, 0.9 cm^3, and 0.5 cm^3, respectively, after modification. The reduction was not statistically significant for D_{max} ($p = 0.24$) or V_{10} ($p = 0.12$), but it was statistically significant for V_{15} ($p = 0.03$; Fig. 4). In all 21 lesions, the average D_{max} was 13.7 Gy (SD 6.53) before modification and 12.0 Gy (SD 6.4) after modification ($p = 0.41$). In total, the V_{10} was 1.8 cm^3 (SD 2.3) before modification and 0.9 cm^3 (SD 1.3) after modification ($p = 0.17$). The V_{15} was 1.3 cm^3 (SD 1.3) before modification and 0.4 cm^3 (SD 0.7) after modification ($p = 0.04$).

In the 15 sets of plans that were modified after seeing the functional information, no statistically significant dose reduction was needed in the PTV. The dose that 95% of the PTV received was 18.5 Gy (SD 4.5) before modification and 17.8 Gy (SD 4.0) after modification ($p = 0.66$). The amount of the PTV receiving ≥80% of the prescribed dose was 4.02 cm^3 (SD 2.15) before modification and 4.02 cm^3 (SD 2.15) after modification ($p = 0.99$; Fig. 4).

In all 21 sets of plans, no reduction was seen in the PTV after modification, as expected. The mean dose that 95% of the PTV received in the 21 plans was 18.4 Gy (SD 4.2) and 17.9 Gy (SD 3.7) before and after the modification ($p = 0.66$). The amount of the PTV receiving ≥80% of the prescribed dose was 5.131 cm^3 (SD 5.27) before and 5.132 cm^3 (SD 5.27) after the modification ($p = 0.99$).

Functional outcome

Adverse events after STI occurred in 4 patients. One patient with AVM had intracranial bleeding and died 3 months after STI (Patient 14). Other adverse events included an increased signal on T_2-weighted MRI in 2 patients (Patients 10 and 13) and radiation necrosis in 1 patient (Patient 4). The former 2 patients did not complain of any neurologic symptoms. The patient with radiation necrosis complained of a minor motor deficit, which showed limitation of movement of the left ankle. This patient had an AVM at the corpus callosum and had undergone MEG but not ADWI before radiosurgery. ADWI was performed when he complained of a motor deficit. It showed radiation injury to the corticospinal pathway (Fig. 5).

DISCUSSION

During the past decade, an increasing body of evidence has indicated that larger doses of radiation lead to better cures of AVM and brain metastases after STI (1, 2, 20, 21). To obtain a cure or local control of disease, coverage of the disease by at least 15 Gy has generally been considered necessary for AVM (1) and ≥18–20 Gy was recommended for brain metastases (20, 21). However, such treatment schedules are consistently accompanied by a 3–7% risk of developing radiation necrosis (1–4, 20, 21). The degree of neurologic deficit is associated with the location and size of the radiation necrosis (3, 4). Therefore, if functional areas are not involved in the high-dose area, patients would be symptom free even if they had radiation necrosis in a silent area. Precise integration of functional images is expected

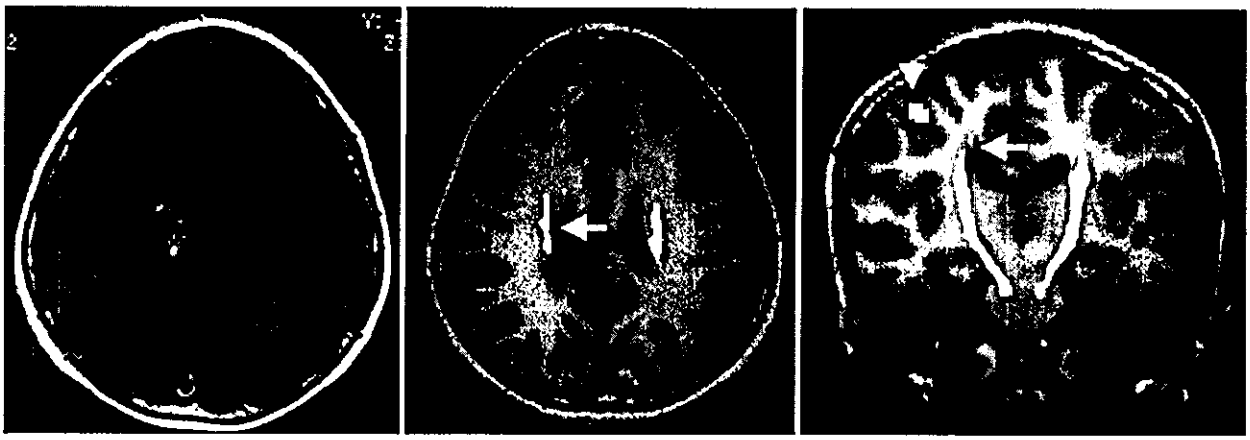

Fig. 5. Magnetic resonance (MR) axonography after radiation necrosis occurred (Patient 4). (a) Enhanced T_1-weighted MRI. (b) axial view of MR axonography. (c) coronal view of MR axonography showing necrotic area (white arrow) involved in right corticospinal tract, which was far from the dipole of the magnetoencephalography image and consistent with the motor cortex (arrowhead).

not only to reduce radiation injury but also to increase the cure rate for AVMs and tumors by allowing delivery of a sufficient dose without fear of adverse reactions.

Apart from MEG, functional MRI (fMRI) and positron emission tomography are reported to be useful functional imaging modalities. fMRI is used for radiotherapy planning (14, 15). MEG provides the direct measure of neuronal electric activity. Compared with MEG, fMRI and positron emission tomography provide a three-dimensional representation of the functional activity in the brain in terms of metabolic and hemodynamic variables. However, the relationship between those variables and neuronal activity has not yet been well defined. Although fMRI can localize the functional cortex, its efficacy and validity for AVMs are reported to be low (13). The major issue is that functional brain mapping by fMRI is based on hemodynamic changes, and thus it might be affected if autoregulation of the blood flow is lost in the brain tissue near the AVM. In contrast, MEG detects the magnetic field associated with intracranial neuronal electric activity itself and thus is not influenced by a high blood flow shunt (13). Therefore, it is reasonable to use MEG in patients with AVMs (13). ADWI, which visualizes the axonal pathway in the brain, has emerged as a potentially useful tool to supplement these images (16–18). Kamiryo *et al.* (13) recently developed a technique combining MEG data and angiography as a tool to provide simultaneous viewing of both modalities in three dimensions. They reported that this technique may reduce the risks associated with embolization treatment (13). A group in New Jersey used fMRI for radiosurgical planning and succeeded in reducing the D_{max} to the functional area in 3 patients in the treatment planning with an average dose reduction of 32% (14, 15).

In the present series, MEG was used in 21 regions in 20 patients to localize the sensorimotor cortex, visual cortex, and Wernicke's area. We also used ADWI in addition to MEG in the 6 most recent patients. Dose–volume histogram analysis revealed that the area of functional brain tissue receiving 15 Gy was significantly reduced when plans were modified after the functional information was provided, and the coverage of the PTV did not significantly deteriorate. One patient with an AVM at the corpus callosum who did not undergo ADWI experienced a minor motor deficit, indicating that functional imaging of the relevant cortex is not sufficient to reduce symptomatic complications. Injury to the corticospinal tract was suggested to be reduced with the use of ADWI.

CONCLUSION

We have developed a method of integrating information about the functional cortex and corticospinal tract into STI planning. Although additional investigation is necessary to understand fully the contribution of functional imaging studies, the results presented here indicate that the integration of functional brain information could potentially reduce the risk of developing neurologic functional disturbance after undergoing STI.

REFERENCES

1. Touboul E, Al Halabi A, Buffat L, *et al.* Single-fraction stereotactic radiotherapy: A dose-response analysis of arteriovenous malformation obliteration. *Int J Radiat Oncol Biol Phys* 1998;41:855–861.
2. Aoyama H, Shirato H, Nishioka T, *et al.* Treatment outcome of single or hypofractionated stereotactic irradiation (STI) using a linear accelerator for intracranial arteriovenous malformation. *Radiother Oncol* 2001;59:323–328.
3. Flickinger JC, Kondziolka D, Lunsford LD, *et al.* Development of a model to predict permanent symptomatic postradiosurgery. *Int J Radiat Oncol Biol Phys* 2000;46:1143–1148.
4. Voges J, Treuer H, Sturm V, *et al.* Risk analysis of linear

radiosurgery. *Int J Radiat Oncol Biol Phys* 1996;36:1055–1063.
5. Kallman P, Agren A, Brahme A. Tumour and normal tissue responses to fractionated non-uniform dose delivery. *Int J Radiat Biol* 1992;62:249–262.
6. Niemierko A, Goitein M. Modeling of normal tissue response to radiation: The critical volume model. *Int J Radiat Oncol Biol Phys* 1992;25:135–145.
7. Fike JR, Cann CE, Turowski K, *et al.* Radiation dose response of normal brain. *Int J Radiat Oncol Biol Phys* 1998;14:63–70.
8. Kamada K, Takeuchi F, Kuriki S, *et al.* Functional neurosurgical stimulation with brain surface magnetic resonance images and magnetoencephalography. *Neurosurgery* 1993;33:269–273.
9. Schulder M, Maldjian JA, Liu WC, *et al.* Functional image-guided surgery of intracranial tumors located in or near the sensorimotor cortex. *J Neurosurg* 1998;89:412–418.
10. Ganslandt O, Fahlbusch R, Nimsky C, *et al.* Functional neuronavigation with magnetoencephalography: Outcome in 50 patients with lesions around the motor cortex. *J Neurosurg* 1999;91:73–79.
11. Kamada K, Kober H, Saguer M, *et al.* Response to silent *Kanji* reading of the native Japanese and German in task subtraction magnetoencephalography. *Cognitive Brain Res* 1998;7:89–98.
12. Alberstone CD, Skirboll SL, Benzel EC, *et al.* Magnetic source imaging and brain surgery: Presurgical and intraoperative planning in 26 patients. *J Neurosurg* 2000;92:79–90.
13. Kamiryo T, Cappell J, Kronberg E, *et al.* Interactive use of cerebral angiography and magnetoencephalography in arteriovenous malformations: Technical note. *Neurosurgery* 2002;50:903–911.
14. Liu WC, Schulder M, Narra V, *et al.* Functional magnetic resonance imaging aided radiation treatment planning. *Med Phys* 2000;27:1563–1572.
15. Shulder M, Vega J, Narra V, *et al.* Functional magnetic resonance imaging and radiosurgical planning. *Stereotact Funct Neurosurg* 1999;73:38–44.
16. Nakada T, Nakayama N, Fujii Y, *et al.* Clinical application of three-dimensional anisotropy contrast magnetic resonance axonography. *J Neurosurg* 1999;90:791–795.
17. Karibe H, Shimizu H, Tominaga T, *et al.* Diffusion-weighted magnetic resonance imaging in the early evaluation of corticospinal tract injury to predict functional motor outcome in patients with deep intracerebral hemorrhage. *J Neurosurg* 2000;95:58–63.
18. Holodny AI, Ollenschleger MD, Liu WC, *et al.* Identification of the corticospinal tracts achieved using blood-oxygen-level-dependent and diffusion functional MR imaging in patients with brain tumors. *AJNR Am J Neuroradiol* 2001;22:83–88.
19. Aoyama H, Shirato H, Nishioka T, *et al.* Magnetic resonance imaging (MRI) system for three-dimensional conformal radiotherapy (3D-CRT) and its impact on gross tumor volume (GTV) delineation of central nervous system (CNS) tumors. *Int J Radiat Oncol Biol Phys* 2001;50:821–827.
20. Shiau CY, Sneed PK, Shu HKG, *et al.* Radiosurgery for brain metastases: Relationship of dose and pattern of enhancement to local control. *Int J Radiat Oncol Biol Phys* 1997;37:375–383.
21. Pirzkall A, Debus J, Lohr F, *et al.* Radiosurgery alone or in combination with whole-brain radiotherapy for brain metastases. *J Clin Oncol* 1998;16:3563–3569.

Acta Neurochir (Wien) (2004) 146: 291–298
DOI 10.1007/s00701-003-0208-x

Acta Neurochirurgica
Printed in Austria

Case Report

Stereotactic radiosurgery for nodular dissemination of anaplastic ependymoma

H. Endo, T. Kumabe, H. Jokura, R. Shirane, and **T. Tominaga**

Department of Neurosurgery, Tohoku University Graduate School of Medicine, Sendai, Japan

Published online February 9, 2004

Summary

Dissemination of primary intracranial ependymoma occurs in 10% of all cases and is difficult to treat, so this may be one of the major reasons for the poor prognosis. Two patients with nodular dissemination of anaplastic ependymoma were treated with repeated stereotactic radiosurgery using the gamma knife (GK), resulting in tumour control over 21 months. GK radiosurgery is a safe and effective treatment option for providing good local control in patients with nodular dissemination of ependymoma.

Keywords: Anaplastic ependymoma; dissemination; gamma knife; stereotactic radiosurgery.

Introduction

Intracranial ependymomas are rare neuro-ectodermal tumours arising from the ependymal cells of the ventricular system, and predominantly occur in children and young adults. Intracranial ependymomas constitute approximately 3% of all intracranial neoplasms and about 10% of all childhood brain tumours [6, 11]. Aggressive multimodality management including surgery, radiation therapy, booster irradiation and chemotherapy have extended the survival time, but the overall survival in most series still does not exceed 60% at 5 years [3, 13, 15, 18]. The pattern of recurrence may be local and/or dissemination to remote sites, and the prognosis after recurrence is quite poor. Dissemination occurs in about 10% of cases of primary intracranial ependymoma [2, 16]. The correlation between prognosis and histological grade of the tumour remains controversial [3, 4, 6, 15, 16, 22], but leptomeningeal dissemination occurs more frequently with high-grade ependymoma than with low-grade ependymoma [16]. The mean survival time after dissemination is 6 months [2].

We treated two patients with anaplastic ependymoma, who manifested multiple nodular dissemination in the course of their disease, by stereotactic radiosurgery (SRS) using the gamma knife (GK). The tumours were controlled for 21 months.

Case reports

Case 1

A 14-year-old girl first presented with headache, nausea and vomiting. She was admitted for treatment of a right lateral ventricular tumour in October 1992. Magnetic resonance (MR) imaging revealed a cystic mass with ring enhancement in the right lateral ventricle, involving the cingulate gyrus (Fig. 1). She underwent subtotal removal of the tumour. Histological examination revealed anaplastic ependymoma. She received 60 Gy of local irradiation and chemotherapy using nimustine hydrochloride (ACNU). She made a complete recovery and radiological study showed no residual tumour. ACNU maintenance therapy was given on an outpatient basis for 1.5 years. She led a normal school life after discharge from our hospital. However, MR imaging performed 4 years and 5 months after the initial treatment revealed a nodular enhanced mass at the cingulate gyrus.

She was treated with GK radiosurgery on four occasions, surgery on three occasions and chemotherapy using cisplatin and etoposide for local recurrences (Table 1). During these treatments, multiple intracranial nodular disseminations occurred. She underwent GK radiosurgery on six occasions for these disseminations in various locations (Table 1, Fig. 2). Fourth ventricular dissemination which first occurred 7 years and 10 months after the initial treatment was treated twice by GK radiosurgery. Although the tumour was controlled for 21 months, MR imaging performed 9 years and 7 months after the initial treatment revealed progression of the tumour. Subtotal removal of the fourth ventricular mass was performed, followed by whole brain irradiation (30 Gy). Follow-up MR imaging performed 9 years and 10 months after

Fig. 1. Case 1: Axial T1-weighted MR image with gadolinium-diethylenetriaminepenta-acetic acid on admission demonstrating a cystic mass with ring enhancement in the right lateral ventricle

the initial treatment showed new dissemination in the anterior horn of the right lateral ventricle, but no enhanced lesion was observed at the primary site and the other nodular disseminations treated by GK radiosurgery were controlled (Fig. 3).

Although the patient developed transient left hemiparesis after the second operation, hemiparesis gradually improved and she began to walk with assistance of mechanical aids. She developed no additional neurological deficits after the third and fourth operations and repeated GK radiosurgery. During these treatments, the patient led a normal school life, entered a nursing school, and passed the national board examination. Her mental status and consciousness was normal, and Karnofsky scale was 70% at the last follow up.

Case 2

A 14-year-old boy presented with headache and nausea persisting for a month. He was admitted for treatment of a fourth ventricular tumour in January 1998. MR imaging revealed a heterogeneous enhanced mass in the fourth ventricle and hydrocephalus (Fig. 4). He underwent subtotal removal of the tumour. Histological examination revealed anaplastic ependymoma. Chemotherapy using cisplatin and etoposide, and local irradiation (33 Gy) by the hyper-fractionated method and craniospinal irradiation (30 Gy) by even-fractionated method were given as adjuvant therapy. Although he suffered from transient lower cranial nerve paresis after the surgery, his neurological condition gradually improved. His first relapse occurred 1 year and 7 months after the initial treatment. MR imaging revealed a small enhanced mass in the fourth ventricle.

GK radiosurgery was performed on three occasions for local recurrence in the fourth ventricle and lower vermis and on three occasions for intracranial nodular dissemination (Table 2, Fig. 5). Multiple nodular disseminations first occurred at 2 years and 4 months after the initial treatment. Nodular dissemination at the thoracic spine occurred 3 years and 10 months after the initial treatment and caused paralysis of the right lower limb and gait disturbance. Surgical removal of the spinal tumour, chemotherapy using ifosfamide, cisplatin and etoposide, and local spinal irradiation (36 Gy) were performed. MR imaging performed 5 months after the surgery showed no residual spinal tumour. MR imaging performed 4 years and 3 months after the initial treatment revealed that the intracranial disseminations were well controlled (Fig. 6). However, follow-up MR imaging performed 4 years and 5 months after the initial treatment revealed diffuse craniospinal dissemination.

During his treatment, the patient led a normal school life and was employed in the computer company after finishing high school. Paraparesis occurred after surgery for the spinal dissemination. His mental status and consciousness was normal, and Karnofsky scale was 60% at the last follow up.

Discussion

The extent of surgical resection is the most consistent factor affecting outcome in cases of intracranial ependymoma [3, 6, 13, 15, 17, 18, 22]. Complete resection can lower the risk of recurrence. The dismal prognosis after recurrence emphasises the importance of the extent of resection at the initial operation. However, complete removal is often not possible and the recurrence rate remains high. The predominant site of relapse is local

Table 1. *Recurrence pattern and treatment for case 1*

Date	Intervals after the initial treatment	Location	Recurrence pattern	Treatment
1992.10.	primary	rt. lateral ventricle of body cingulate gyrus	primary	subtotal removal, LB (60 Gy), ACNU
1997.8.	4 y 5 mo	cingulate gyrus	local 1	GK (25 Gy)
1998.10.	5 y 5 mo	cingulate gyrus	local 2	total removal, CDDP + VP-16
1999.2.	5 y 11 mo	cingulate gyrus	local 3	GK (16 Gy)
1999.10.	6 y 7 mo	cingulate gyrus	local 4	total removal
2000.3.	7 y	cingulate gyrus	local 5	GK (18 Gy)
2001.1.	7 y 10 mo	cingulate gyrus fourth ventricle	local 6 dissemination 1	GK (22 Gy) GK (22 Gy)
2001.2.	7 y 11 mo	cingulate gyrus	local 7	total removal
2001.12.	8 y 9 mo	rt. trigone	dissemination 2	GK (22 Gy)
2002.1.	8 y 10 mo	fourth ventricle	dissemination 3	GK (23 Gy)
2002.5.	9 y 2 mo	septum pellucidum	dissemination 4	GK (23 Gy)
2002.8.	9 y 5 mo	lt. lateral ventricle of body rt. trigone	dissemination 5 dissemination 6	GK (23 Gy) GK (22 Gy)
2002.12.	9 y 9 mo	fourth ventricle	dissemination 7	subtotal removal, WB (30 Gy)

GK Gamma knife radiosurgery; *LB* local brain irradiation; *CDDP* cisplatin; *VP-16* etoposide; *WB* whole brain irradiation.

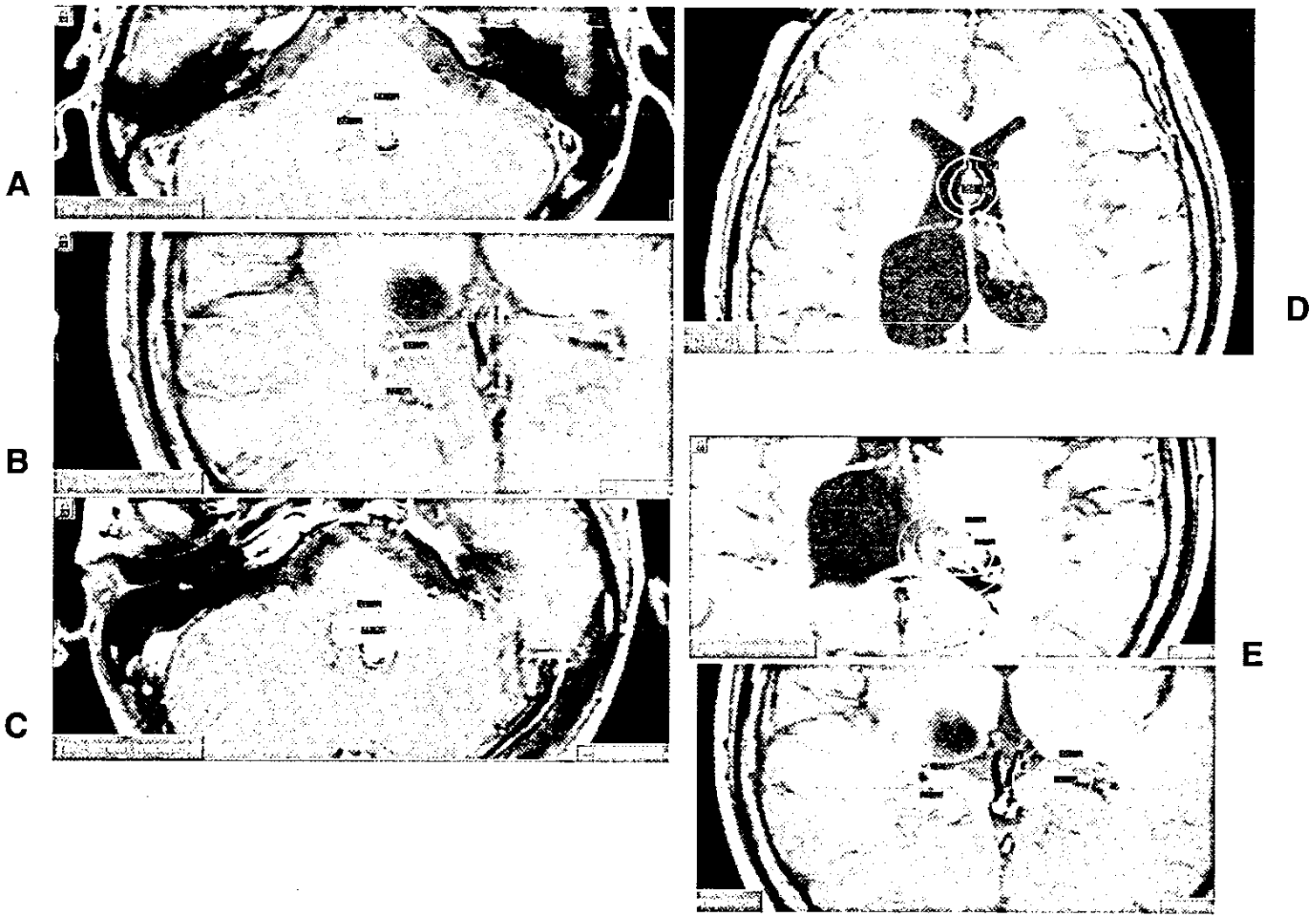

Fig. 2. Case 1: Axial T1-weighted MR images with gadolinium-diethylenetriaminepenta-acetic acid displayed on workstations running the Leksell GammaPlan program. (A) First Gamma knife (*GK*) radiosurgery for fourth ventricular dissemination. (B) First GK radiosurgery for dissemination in the right trigone. (C) Second GK radiosurgery for fourth ventricular dissemination. (D) GK radiosurgery for dissemination in the septum pellucidum. (E) Second GK radiosurgery for dissemination in the right trigone and GK radiosurgery for left lateral ventricular dissemination

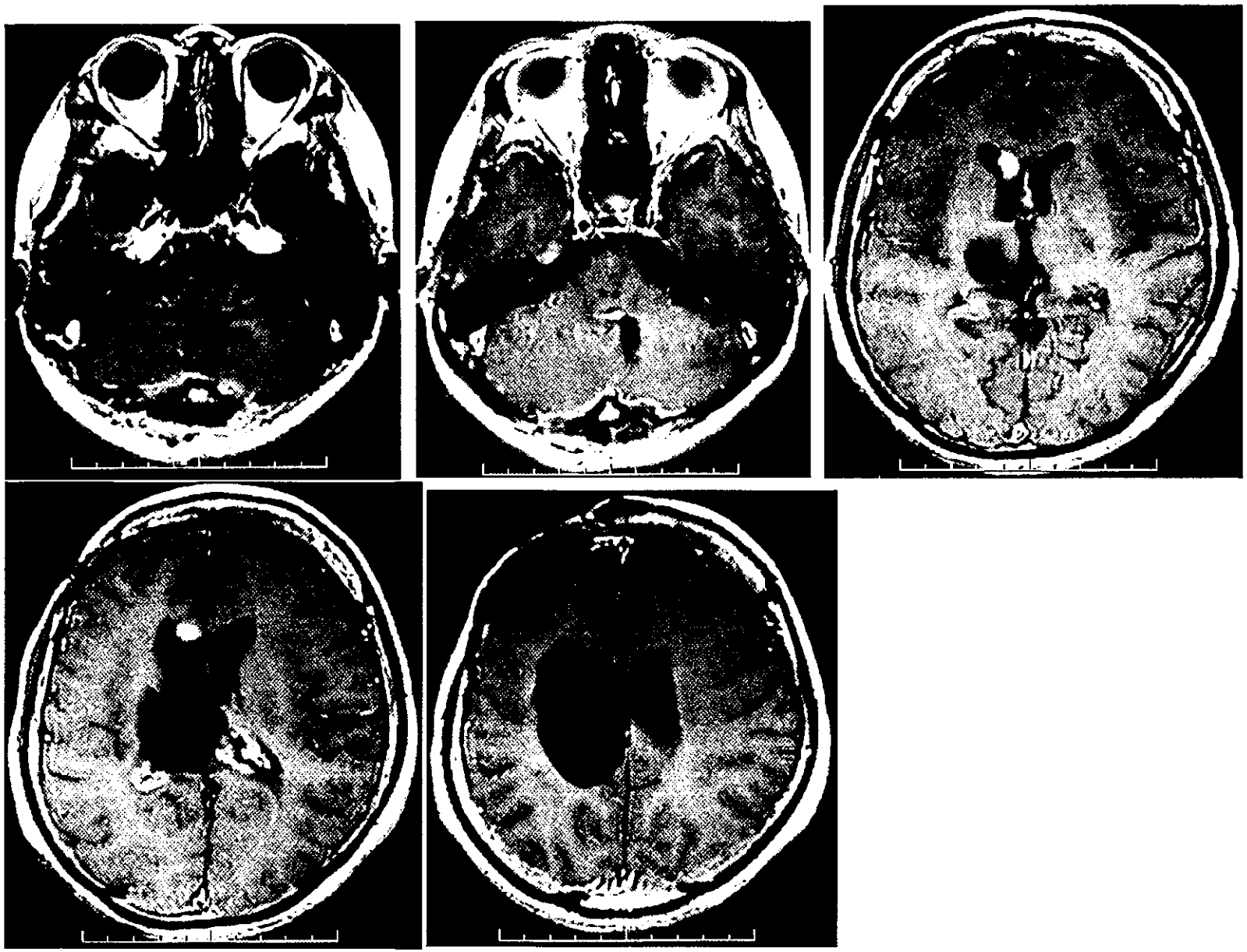

Fig. 3. Case 1: Last follow-up axial T1-weighted MR images with gadolinium-diethylenetriaminepenta-acetic acid performed 9 years and 10 months after the initial treatment showing good control of the primary tumour and multiple nodular disseminations treated by Gamma knife radiosurgery, but new dissemination in the anterior horn of the right lateral ventricle

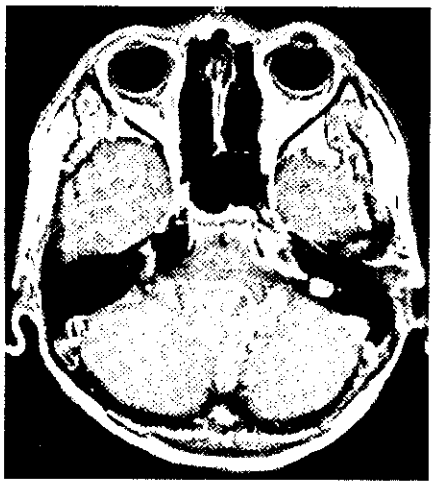

Fig. 4. Case 2: Axial T1-weighted MR image with gadolinium-diethylenetriaminepenta-acetic acid on admission demonstrating a heterogeneous enhanced mass in the fourth ventricle

[19, 20, 23], and postoperative local field irradiation is very suitable for adjuvant therapy [13]. A retrospective study of nondisseminated infratentorial ependymoma suggested that the tumour bed and a safety margin should be the target volume instead of the entire posterior fossa [14].

Dissemination is another important pattern of recurrence in cases of ependymoma. Advances in surgical techniques and adjuvant therapy can control the tumour locally and prolong mean survival time, but the occurrence of dissemination becomes more likely. Dissemination without local recurrence is rare [12]. The incidence of dissemination for primary intracranial ependymoma is about 10% [2, 16]. The high-grade and myxopapillary subtypes are associated with dissemination [16]. Craniospinal irradiation has been advocated for high-grade ependymoma to prevent dissemination [19], but such treatment is not considered as standard.

SRS is effective as a boost after conventional radiation therapy or for the treatment of recurrent disease [1, 5, 7, 8, 10, 21]. Treatment of 22 patients with progressive anaplastic ependymoma using GK radiosurgery as a boost resulted in a median survival time after radiosurgery of 2.2 years and distant recurrence in 9 patients (40.9%) at a mean of 10 months [8]. Treatment of 12 patients with recurrent ependymoma resulted in local control in 68% at 3 years, but two patients suffered distant metastasis, indicating that SRS provided good local tumour control, but dissemination remained an important problem [21].

Treatment of patients with recurrent disseminated ependymomas by SRS has not been reported before. Dissemination may occur in diffuse or loculated patterns [9], and SRS may be indicated for the loculated pattern. The nodular pattern of leptomeningeal dissemination is less common than the diffuse pattern. Medulloblastoma is the most frequent underlying primary tumour to cause nodular dissemination [9]. In our experience, anaplastic ependymomas also tend to cause nodular dissemination, which can be controlled by SRS. Repeated GK radiosurgery controlled nodular disseminated anaplastic ependymoma for 21 months without neurotoxicity in our two patients. Among six previous cases of disseminated ependymoma, one patient received no treatment for dissemination, three were treated with radiation therapy and two were treated with chemotherapy [2]. The mean survival time after the treatment of dissemination was 6 months [2]. Considering that our two patients were still alive at last follow up and the disseminated tumour was controlled for more than 21 months, SRS seems to be effective in the treatment of dissemination. Beyond the first relapse, there is little hope for long-term survival with conventional therapy [4]. Although SRS is not the treatment to cure the disease, it might be the

Table 2. *Recurrence pattern and treatment for case 2*

Date	Intervals after the initial treatment	Location	Recurrence pattern	Treatment
1998.1.	primary	fourth ventricle	primary	subtotal removal, LB (33 Gy), WB & WS (30 Gy), CDDP + VP-16
2000.4.	1 y 8 mo	fourth ventricle	local 1	GK (18 Gy)
2000.11.	2 y 3 mo	vermis	local 2	GK (18 Gy)
2000.12.	2 y 4 mo	corpus callosum	dissemination 1	GK (22 Gy)
2001.8.	3 y	fourth ventricle	local 3	GK (20 Gy)
2001.12.	3 y 4 mo	corpus callosum	dissemination 2	GK (22 Gy)
2002.5.	3 y 9 mo	rt. lateral ventricle of body	dissemination 3	GK (25 Gy)
2002.6.	3 y 10 mo	spinal cord (T7-9)	dissemination 4	subtotal removal, LS (36 Gy), IFOS + CDDP + VP-16

GK Gamma knife radiosurgery; *LB* local brain irradiation; *WB & WS* whole brain & whole spine irradiation; *CDDP* cisplatin; *VP-16* etoposide; *T* thoracic spine; *LS* local spine irradiation; *IFOS* ifosfamide.

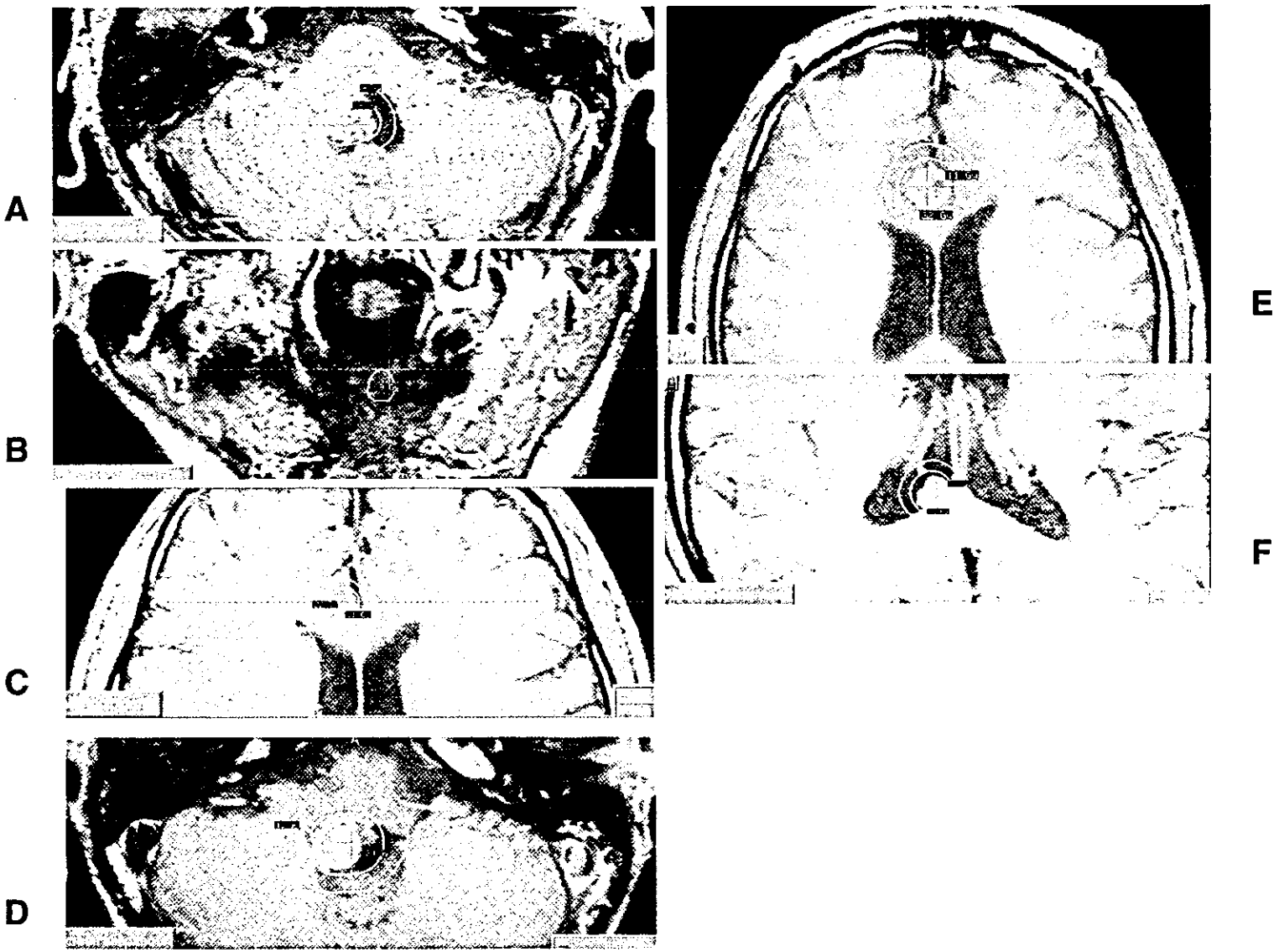

Fig. 5. Case 2: Axial T1-weighted MR images with gadolinium-diethylenetriaminepenta-acetic acid displayed on workstations running the Leksell GammaPlan program. (A) First Gamma knife (*GK*) radiosurgery for local recurrence. (B) Second GK radiosurgery for local recurrence. (C) First GK radiosurgery for dissemination in the corpus callosum. (D) Third GK radiosurgery for local recurrence. (E) Second GK radiosurgery for dissemination in the corpus callosum. (F) GK radiosurgery for dissemination in the right lateral ventricle

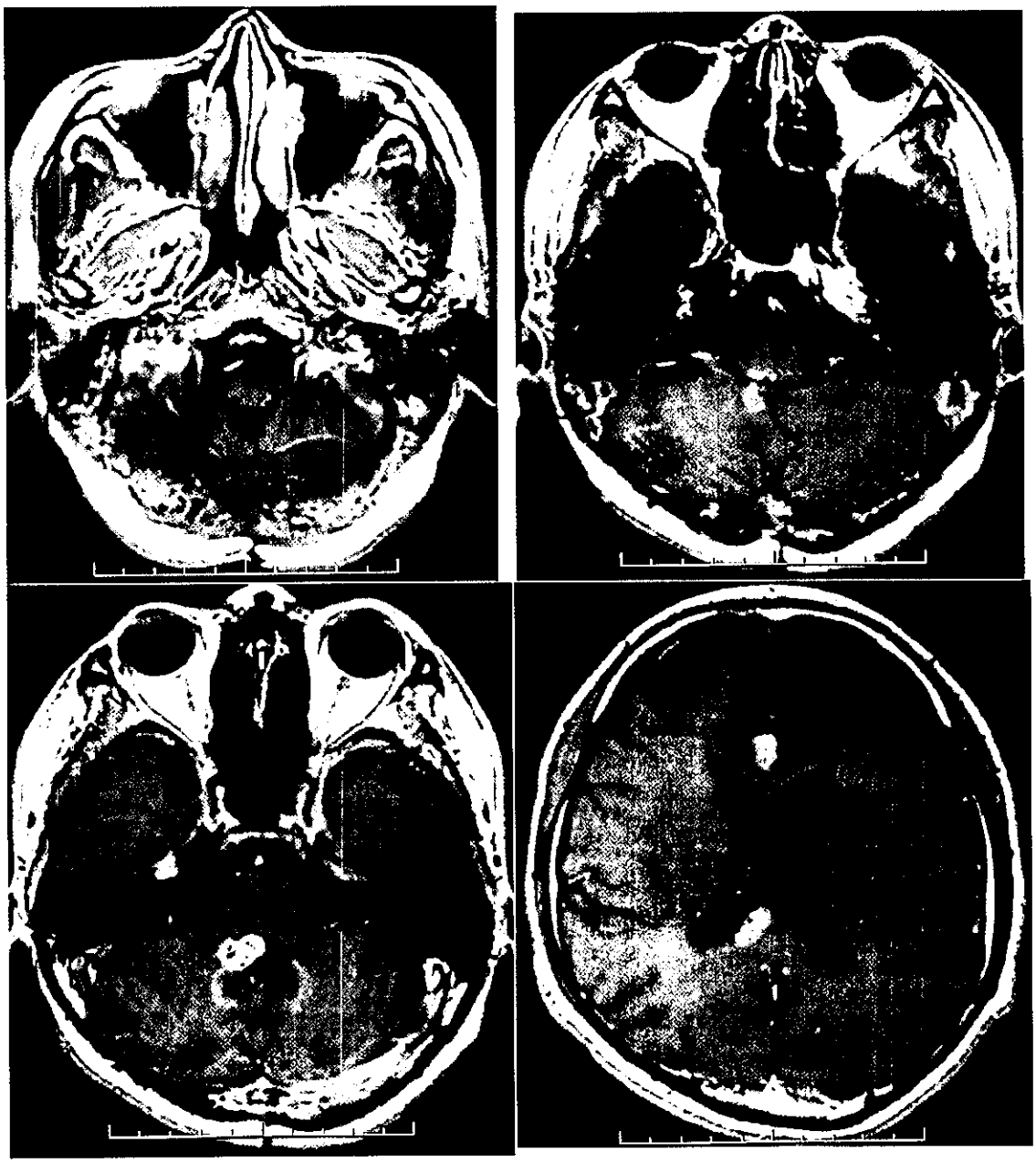

Fig. 6. Case 2: Axial T1-weighted MR images with gadolinium-diethylenetriaminepenta-acetic acid performed 4 years and 3 months after the initial treatment showing nodular enhanced masses in the fourth ventricle, vermis, right lateral ventricle, and corpus callosum

treatment of choice if the patient could benefit from aggressive treatment.

Conclusion

Dissemination is the final form of ependymoma and is difficult to treat. GK radiosurgery can provide safe and effective local control in patients with nodular dissemination of ependymoma. In addition, GK radiosurgery can be repeated because of its minimal neurotoxicity. Although out-of-field tumour progression remains a problem, GK radiosurgery may be the treatment of choice for patients with nodular dissemination.

References

1. Aggarwal R, Yeung D, Kumar P, Muhlbauer M, Kun LE (1997) Efficacy and feasibility of stereotactic radiosurgery in the primary management of unfavorable pediatric ependymoma. Radiother Oncol 43: 269–273
2. Calvo FA, Hornedo J, De La Torre A, Sachetti A, Arellano A, Aramburo P, Aragon G, Otero J (1983) Intracranial tumors with risk

of dissemination in neuroaxis. Int J Radiat Oncol Biol Phys 9: 1297–1301
3. Figarella-Branger D, Civatte M, Bouvier-Labit C, Gouvernet J, Gambarelli D, Gentet JC, Lena G, Choux M, Pellissier JF (2000) Prognostic factors in intracranial ependymomas in children. J Neurosurg 93: 605–613
4. Goldwein JW, Glauser TA, Packer RJ, Finlay JL, Sutton LN, Curran WJ, Lachy JM, Rorke LB, Schut L, D'Angio GJ (1990) Recurrent intracranial ependymomas in children. Cancer 66: 557–563
5. Grabb PA, Lunsford LD, Albright AL, Kondziolka D, Flickinger JC (1996) Stereotactic radiosurgery for glial neoplasms of childhood. Neurosurgery 38: 696–701
6. Healey EA, Barnes PD, Kupsky WJ, Scott RM, Sallan SE, Black PM, Tarbell NJ (1991) The prognostic significance of postoperative residual tumor in ependymoma. Neurosurgery 28: 666–672
7. Hirato M, Nakamura M, Inoue HK, Ohye C, Hirato J, Shibazaki T, Andou Y (1995) Gamma knife radiosurgery for the treatment of brain stem tumors. Stereotact Funct Neurosurg 64 [Suppl 1]: 32–41
8. Jawahar A, Kondziolka D, Flickinger JC, Lunsford LD (1999) Adjuvant stereotactic radiosurgery for anaplastic ependymoma. Stereotact Funct Neurosurg 73: 23–30
9. Lee YY, Tien RD, Bruner JM, De Pena CA, Van Tassel P (1989) Loculated intracranial leptomeningeal metastasis: CT and MR characteristics. AJNR Am J Neuroradiol 10: 1171–1179
10. Loeffler JS, Rossitch E Jr, Siddon R, Moore MR, Rockoff MA, Alexander E III (1990) Role of stereotactic radiosurgery with a linear accelerator in treatment of intracranial arteriovenous malformations and tumors in children. Pediatrics 85: 774–782
11. Miller RW, Young JL, Novakovic B (1994) Childhood cancer. Cancer 75: 395–405
12. Nakasu S, Ohashi M, Suzuki F, Matsuda M (2001) Late dissemination of fourth ventricle ependymoma: a case report. J Neurooncol 55: 117–120
13. Nazar GB, Hoffman HJ, Becker LE, Jenkin D, Humphreys RP, Hendrick EB (1990) Infratentorial ependymomas in childhood: prognostic factors and treatment. J Neurosurg 72: 408–417
14. Paulino AC (2001) The local field in infratentorial ependymoma: does the entire posterior fossa need to be treated? Int J Radiat Oncol Biol Phys 49: 757–761
15. Pollack IF, Gerszten PC, Martinez AJ, Lo KH, Shultz B, Albright AL, Janosky J, Deutsch M (1995) Intracranial ependymomas of childhood: long-term outcome and prognostic factors. Neurosurgery 37: 655–667
16. Rezai AR, Woo HH, Lee M, Cohen H, Zagzag D, Epstein FJ (1996) Disseminated ependymoma of the central nervous system. J Neurosurg 85: 618–624
17. Robertson PL, Zeltzer PM, Boyett JM, Rorke LB, Allen JC, Geyer JR, Stanley P, Li H, Albright AL, McGuire-Cullen P, Finlay JL, Stevens KR Jr, Milstein JM, Packer RJ, Wisoff J (1998) Survival and prognostic factors following radiation therapy and chemotherapy for ependymomas in children: a report of the Children's Cancer Group. J Neurosurg 88: 695–703
18. Rousseau P, Habrand JL, Sarrazin D, Kalifa C, Terrier-Lacombe MJ, Rekacewicz C, Rey A (1994) Treatment of intracranial ependymomas of children: review of a 15-year experience. Int J Radiat Oncol Biol Phys 28: 381–386
19. Salazar OM, Castro-Vita H, VanHoutte P, Rubin P, Aygun C (1983) Improved survival in cases of intracranial ependymoma after radiation therapy. Late report and recommendations. J Neurosurg 59: 652–659
20. Shaw EG, Evans RG, Scheithauer BW, Ilstrup DM, Earle JD (1987) Postoperative radiotherapy of intracranial ependymoma in pediatric and adult patients. Int J Radiat Oncol Biol Phys 13: 1457–1462
21. Stafford SL, Pollack BE, Foote RL, Gorman DA, Nelson DF, Schomberg PJ (2000) Stereotactic radiosurgery for recurrent ependymoma. Cancer 88: 870–875
22. van Veelen-Vincent ML, Pierre-Kahn A, Kalifa C, Sainte-Rose C, Zerah M, Thorne J, Renier D (2002) Ependymoma in childhood: prognostic factors, extent of surgery, and adjuvant therapy. J Neurosurg 97: 827–835
23. Wallner KE, Wara WM, Sheline GE, Davis RL (1986) Intracranial ependymomas: results of treatment with partial or whole brain irradiation without spinal irradiation. Int J Radiat Oncol Biol Phys 12: 1937–1941

Comments

1. This paper describes an aggressive treatment strategy for two patients with disseminated ependymoma. I admire the authors' enthusiasm, but I find it difficult to recommend this treatment strategy in general.
2. The best-documented treatment of ependymoma is total tumour resection. In my opinion craniospinal radiotherapy is not indicated as part of the primary treatment, since less than 10% of ependymoma patients get dissemination. If radiotherapy is given as part of primary treatment, it should be focal.
3. Disseminated ependymoma has a dismal prognosis. Aggressive treatment of these patients with radiotherapy, chemotherapy or surgery, can at best give a short increase in patient survival with good quality of life. Most patients with disseminated ependymoma would probably not benefit from aggressive treatment.

Eirik Helseth

The authors studied and described well the efficacy of stereotactic radiosurgery for recurrent disseminated nodular ependymomas. Those tumours are apparently difficult to treat well, and stereotactic radiosurgery might be the best therapeutic option today.

Kintomo Takakura

Correspondence: Toshihiro Kumabe, M.D., Department of Neurosurgery, Tohoku University Graduate School of Medicine, 1-1 Seiryo-machi, Aoba-ku, Sendai 980-8574, Japan. e-mail: kuma@nsg.med.tohoku.ac.jp

Acta Neurochir (Wien) (2004) 146: 251–255
DOI 10.1007/s00701-003-0191-2

Acta Neurochirurgica
Printed in Austria

Clinical Article

Routine clinical adoption of magnetic resonance imaging was associated with better outcome after surgery in elderly patients with a malignant astrocytic tumour: a retrospective review

M. Fujimura, T. Kumabe, T. Tominaga, H. Jokura, R. Shirane, and **T. Yoshimoto**

Department of Neurosurgery, Tohoku University Graduate School of Medicine, Sendai, Japan

Published online January 8, 2004

Summary

Background. There is controversy about extensive surgical treatment for a malignant astrocytic tumour in more elderly patients who may have poorer outcomes and higher complication rates. This retrospective study investigated outcome in elderly patients with malignant astrocytic tumour before and after the adoption of routine clinical use of magnetic resonance (MR) imaging.

Methods. During 1982 through 1999, 88 patients with malignant astrocytic tumour aged 60 years or over were treated in our institute. Thirty-seven patients had an anaplastic astrocytoma and 51 had a glioblastoma. Thirty-seven patients treated from 1982 to 1988 did not have pre-operative evaluation by MR imaging (Group A), 26 patients treated from 1989 to 1995 had preoperative MR imaging evaluation (Group B), and 25 patients treated after 1996 underwent preoperative MR imaging with functional brain mapping and intra-operative navigation system monitoring (Group C).

Findings. The median survival time was 8.8 months in Group A, 12.7 months in Group B, and 17.6 months in Group C. Patients with glioblastoma in Group B (11.7 months, $n = 15$) and Group C (16.0 months, $n = 19$) had significantly longer median survival time than in Group A (6 months, $n = 17$) ($P = 0.0054$ between Groups A and B, $P = 0.0024$ between Groups A and C). Better preoperative performance status, more thorough surgical resection, and better performance status after the initial treatment was obtained after the introduction of MR imaging, and patients with the optimal indicators showed significantly longer survival time compared with the patients without these factors.

Interpretation. Pre-operative MR imaging may contribute to longer survival time by providing an earlier diagnosis in patients with better performance status, by allowing more thorough surgical resection, and resulting in better performance status after the treatment.

Keywords: Malignant astrocytoma; elderly; outcome; surgery.

Introduction

The treatment of patients with a malignant astrocytic tumour is one of the most challenging contemporary neurosurgical problems. Surgical treatment, especially for the elderly, is considered to result in a poor outcome and a high complication rate [3, 7, 8]. The median survival was only 2.2 months in patients older than 60 years with glioblastoma [9]. Craniotomy plus radiotherapy improved the median survival up to 16 weeks in elderly patients (60 years or over) who were treated during 1983 through 1989 [14]. In a series of 146 adults, 27 were older than 65 years and had a median survival of only 4.8 months [6]. These reports illustrate the poor prognosis for elderly patients with malignant astrocytic tumour.

Total surgical resection with adjuvant radiochemotherapy is considered to be optimal leading to prolonged survival time and improved neurological status in patients with a malignant astrocytic tumour [12]. However, the merits of extensive surgical resection in elderly patients with a malignant astrocytic tumour, remain controversial [8]. Extensive or repeated surgery in an elderly patient may have greater risks of surgical morbidity and death and there are several reports that radical surgery provides little benefit for elderly patients with a malignant astrocytic tumour [5, 7]. Nevertheless, in another report the optimal results in elderly patients were achieved in those in better performance status by thorough surgical resection and definitive radiation therapy [10].

The present study is based on a comprehensive analysis of the medical records in our department during 1982 through 1999 in order to assess the outcome in elderly patients with a malignant astrocytic tumour

before and after the introduction of magnetic resonance (MR) imaging. We analyzed the prognostic importance of pre- and postoperative performance status, extent of surgical resection at operation, and postoperative complications.

Methods and material

Case material

During 1982 through 1999, 281 patients with malignant astrocytic tumour were treated by surgical procedures and/or radio-chemotherapy in our department. One hundred and seven patients treated from 1982 to 1988 had no pre-operative evaluation by MR imaging (Group A), 84 patients from 1989 to 1995 underwent pre-operative MR imaging evaluation (Group B), and 90 patients after 1996 underwent preoperative MR imaging including functional brain mapping and surgery under guidance from an intra-operative navigation system (Group C). Intra-operative functional mapping was also used for patients with malignant astrocytic tumour in eloquent areas in Group C.

The present study included 88 patients who were aged 60 years or over. The 51 male and 37 female patients were aged from 60 to 78 years (mean age 66.8 ± 4.7 years). Twenty-seven patients were older than 70 years. There were 37 patients in Group A, 26 patients in Group B, and 25 patients in Group C.

Histological confirmation was required for inclusion in this study. The histological diagnosis was established using the new World Health Organization classification. The 281 patients with malignant astrocytic tumour included 154 cases of anaplastic astrocytoma and 127 cases of glioblastoma. Thirty-seven (24.0%) of the cases of anaplastic astrocytoma, and 51 (40.2%) of the cases of glioblastoma occurred in elderly patients.

Treatment

The treatment protocol was relatively uniform but not identical for all patients. Thirty patients (34.1%) underwent gross total resection, and 58 patients (65.9%) underwent partial resection or stereotactic biopsy. Nineteen patients were treated by radiation therapy. The standard radiation therapy consisted of 30 Gy in 15 fractions to the tumour and peritumoral brain and 30 Gy in 15 fractions to the whole brain before 1987, and 60 Gy in 30 fractions to the local brain thereafter. The standard radiotherapy protocol was a total dose of 60 Gy in 30 fractions of 2 Gy, 5 days per week over 6 weeks, delivered to the local brain by parallel opposed ports with megavoltage equipment. 1-(4-Amino-2-methyl-5-pyrimidinyl) methyl-3-(2-chloroethyl)-3-nitrosourea (ACNU) was administered intravenously or intra-arterially for 58 patients.

Clinical investigation

The pre- and postoperative performance status was classified using the Eastern Co-operative Oncology Group (ECOG) scale ranging from 0 to 4. The postoperative performance status was determined between 1 and 3 months after surgery. Surgical morbidity was defined as postoperative intracranial haematoma, iatrogenic neurological deficit, and sepsis at the surgical site. Follow-up analysis was obtained by review of the patient's records or by contact with the family. Eighty-three of the 88 patients (94.3%) had died by the cut-off date for data analysis, June 30, 2001. For survival analysis, day 0 was defined as the first day of admission.

Statistical analysis

Survival rates were determined using the Kaplan-Meier method. The statistical significance between life table curves was determined using the logrank test.

Results

The median survival time of the 88 elderly patients was 11.7 months, which was significantly shorter than that of patients under the age of 60 years. Median survival times of the elderly patients with anaplastic astrocytoma and glioblastoma were significantly shorter than those of the younger patients with these tumours. The median survival time of elderly patients with anaplastic astrocytoma was significantly longer than that of elderly patients with glioblastoma (Table 1).

As shown in Table 2, median survival times of elderly patients with glioblastoma in Groups B (11.7 months, $n = 15$) and C (16.0 months, $n = 19$) were significantly longer than those in Group A (6 months, $n = 17$), respectively ($p = 0.0054$ between A and B, $p = 0.0024$ between A and C). Median survival time was somewhat longer after the introduction of functional brain mapping and

Table 1. *Survival in patients undergoing surgery for malignant astrocytic tumour*

Histology	No. of patients	Median survival time (months)	Probability
Total	281		
–under 60 year	193	22.6	P < 0.0001
–60 year or over	88	11.7	
Anaplastic astrocytoma	154		
–under 60 years	117	29.3	P = 0.0006
–60 years or over	37	14.7*	
Glioblastoma	127		
–under 60 years	76	16.3	P = 0.0021
–60 years or over	51	10.8*	

* P = 0.0105.